www.czasopisma.pan.pl www.journals.pan.pl
Chemical and Process Engineering 2016, 37 (3), 441-457
DOI: 10.1515/cpe-2016-0037

ANALYSIS OF THE MECHANISM OF GAS BUBBLE BREAK-UP IN LIQUIDS DURING THE SELF-ASPIRATING IMPELLER OPERATION

Jacek Stelmach, Czesław Kuncewicz*, Radosław Musoski

Lodz University of Technology, Faculty of Process and Environmental Engineering, ul. Wólczańska 213, 90-924 Łódź, Poland

Feasibility of a model of gas bubble break-up and coalescence in an air-lift column enabling determination of bubble size distributions in a mixer with a self-aspirating impeller has been attempted in this paper. According to velocity measurements made by the PIV method with a self-aspirating impeller and Smagorinski's model, the spatial distribution of turbulent energy dissipation rate close to the impeller was determined. This allowed to positively verify the dependence of gas bubble velocity used in the model, in relation to turbulent energy dissipation rate. Furthermore, the range of the eddy sizes capable of breaking up the gas bubbles was determined. The verified model was found to be greatly useful, but because of the simplifying assumptions some discrepancies of experimental and model results were observed.

Keywords: self-aspirating impeller, PIV, gas bubble size distribution, energy dissipation rate, gas bubble sizes

1. INTRODUCTION

Mechanical mixing with simultaneous dispersion of gas in liquid is often used in industrial plants where a direct contact of liquid with gas is required. In a closed vessel, apart from traditional solutions using a sparger, to reach gas recirculation we can use self-aspirating impellers. However, so far the process of gas dispersion by self-aspirating impellers has not been thoroughly investigated. It was found out (Deshmukh et al., 2006; Evans et al., 1992; Patil and Joshi, 1999; Patwardahan and Joshi, 1999; Stelmach, 2000) that the gas stream dispersed by self-aspirating impellers depends on hydrostatic pressure of the liquid column over the impeller and on its rotational frequency. The onset of gas dispersion is usually determined by a critical value of modified Froude number (Deshmukh et al., 2006; Forrester et al., 1998; Patwardahan and Joshi, 1999; Wang et al., 2013).

$$Fr' = \frac{N^2 \cdot D^2}{g \cdot (H - h)} \tag{1}$$

For the self-aspirating disc impeller, a value of $Fr'_{cr} = 0.207$ was experimentally obtained (Stelmach, 2000). This value is consistent with literature data for impellers exhibiting a similar mode of operation, according to which $Fr'_{cr} = 0.21 \pm 0.04$ (Ju et al., 2009; Poncin et al., 2002; Sardeindg et al., 2006)

At the onset of self-aspiration, when the Fr'_{cr} value is exceeded, the gas stream and bubble number are quite insignificant and gas bubbles only minimally disturb the system hydrodynamics. This phase of gas dispersion is presented in Fig. 1. Photos show bubbles flowing out of the orifices for the same blade position in different random times.

*Corresponding author, e-mail: czeslaw.kuncewicz@p.lodz.pl

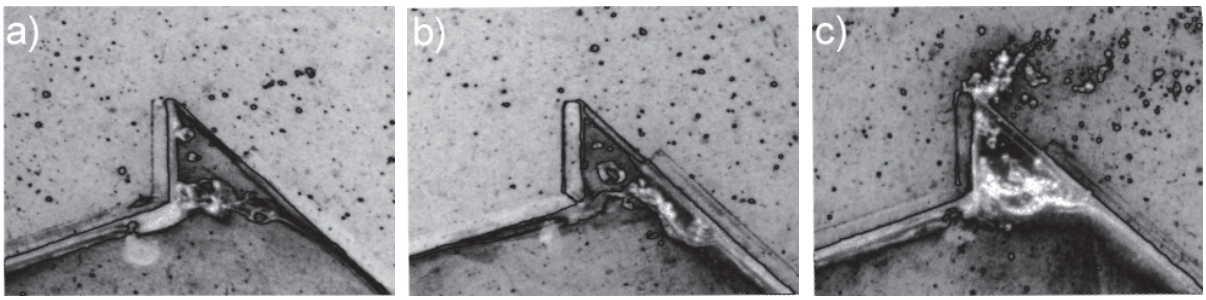

Fig. 1. Outflow of gas for $D = 0.125$ m, $H = 0.3$ m, $N = 6$ s^{-1} and $Fr' = 0.253$ (Stelmach, 2006)

At this stage of self-aspiration even a slight increase in the impeller rotational frequency results in an increase of gas flow. This can be seen by comparing Fig. 1 with Fig. 2.

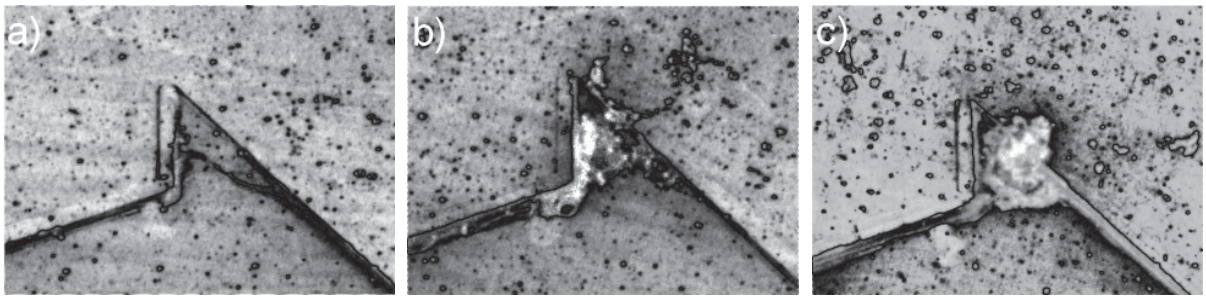

Fig. 2. Outflow of gas for $D = 0.125$ m, $H = 0.3$ m, $N = 6.08$ s^{-1} and $Fr' = 0.260$ (Stelmach, 2006)

As indicated by analysis of both figures, gas outflow from the impeller looks like formation of bubbles at the cross-flow of liquid in relation to the orifice (Forrester and Rielly, 1998; Kulkarni and Joshi, 2005; Tan et al., 2000; Zhang and Shoji, 2001; Zhang and Tan, 2000). The impeller blades actually do not take any part in bubble breaking-up, which is the main mechanism of breaking-up in the case of gas supply under the impeller blades by sparger or nozzle. In this case the breaking-up takes place mostly in the turbulent field just behind the impeller blade. In the impeller outlet there is a gas cavern the end of which, in form of a gas tail, is broken up into smaller bubbles. The broken up bubbles may undergo further breakdown in the turbulent field. In most processes taking place in the liquid-gas system, while the bubbles collide inside the mixer, they may also undergo coalescence (Laakkonen et al., 2002). Because of minimal participation of the impeller blades in bubble break-up, there is a similarity between gas breaking-up mechanism in the mixer with the self-aspirating impeller and breaking-up in the air-lift column.

Gas bubble sizes belong to the most important process parameters conditioning the rate of the mass transfer during aeration. Because of short presence of large bubbles, not all the oxygen diffuses from bubbles to liquid. On the other hand, from small bubbles all the oxygen they contain can very fast penetrate the liquid and their further stay in the liquid comprising only inert gas is pointless. Therefore, the possibility to determine the bubble size at the mixer designing stage is very important. Eddy sizes change both in time and space. Eddy sizes are mostly connected with the local energy dissipation rate inside the mixer (Luo and Svendsen, 1996; Martínez-Bazán et al., 1999a; Laakkonen et al., 2007). According to the dispersed systems theory, it is the so-called small eddies, i.e. the eddies of size approximately the same as that of bubbles, that decide whether the gas bubble will be broken up or not (Stręk, 1981). So there should be a correlation between bubble sizes and sizes of eddies generated by the impeller. It is difficult to determine directly eddy sizes in the whole mixer, therefore they are often determined using the mean energy dissipation rate value. This parameter is particularly useful in calculations of the Sauter mean diameter. It can usually be calculated from the equation of the following type (Martín et al., 2008a; Martín et al., 2008b)

$$d_{32} = C_1 \frac{\sigma^{3/5}}{\rho^{3/5} \cdot \varepsilon_m^{2/5}} \tag{2}$$

where ε_m is a power consumption related to the mass unit, and coefficient C_1 has a value close to unity. Based on Eq. (2), many relationships were developed for various types of liquids (Kawase and Moo-Young, 1990). Besides, the Eq. (3) with the critical value of Weber number We_C is used (Rigby et al., 1997)

$$d_{32} = C_2 \cdot \varepsilon_m^{-\frac{2}{5}} \cdot \left(\frac{We_C \cdot \sigma}{2 \cdot \rho} \right)^{\frac{3}{5}} \tag{3}$$

The Sauter diameter is used in calculations of the mass transfer process. However, it does not give any precise information about the bubble size distribution, i.e. how much the distribution differs from the monodispersive system. In our previous research related to operation of the self-aspirating disc impeller (Stelmach, 2006; Stelmach, 2007), we determined the air bubble size distributions dispersed in water at the impeller level for values *Fr'* only slightly higher than the critical value. The obtained results are shown in Fig. 3.

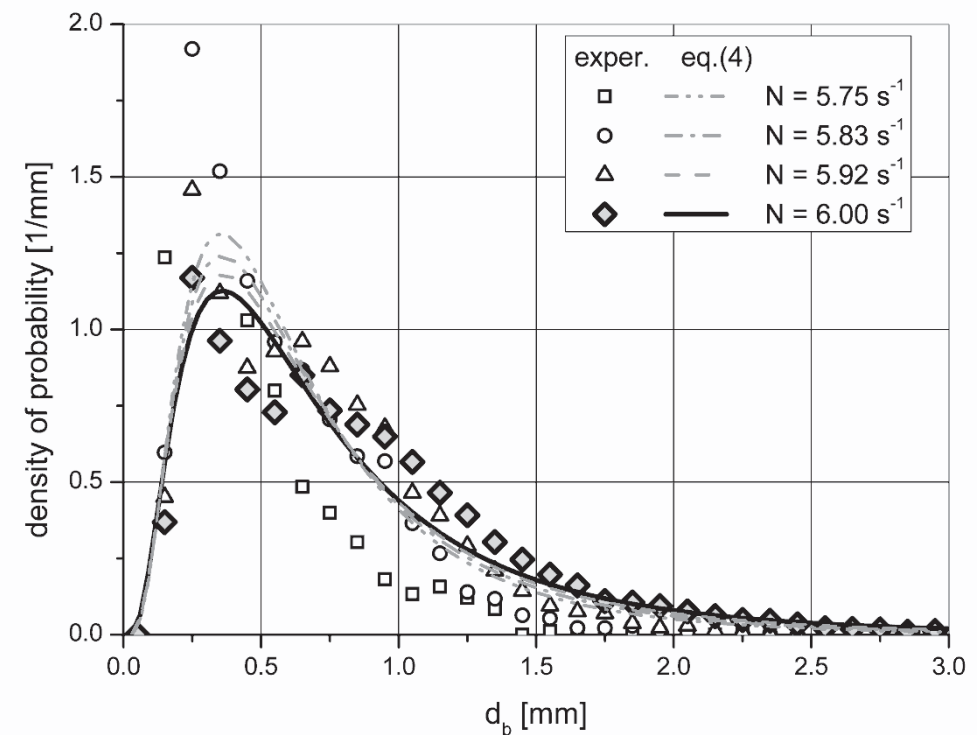

Fig. 3. Bubble diameter distribution (Stelmach, 2007)

It was concluded that the air bubble size probability density distributions in water are well described by the logarithmic normal distribution (Stelmach, 2007)

$$f(x) = \frac{1}{x \cdot \sigma_x \cdot \sqrt{2 \cdot \pi}} exp\left[- \frac{(ln\, x - \mu_x)^2}{2 \cdot \sigma_x^2} \right] \tag{4}$$

where

$$\mu_x = -0.0089 \cdot Fr'^{-2.455} \cdot \left(\frac{H-h}{T} \right)^{-0.759} \cdot \left(\frac{D}{T} \right)^{-0.453} \tag{5}$$

$$\sigma_x = \frac{4.391 \cdot Fr' - 0.079}{\left(\frac{H-h}{T}\right)^{-0.134} \cdot \left(\frac{D}{T}\right)^{-0.338}} \tag{6}$$

Solid lines in Fig. 3 are depicted according to Eqs. (4) and (5).

As we have mentioned, literature includes information about gas bubble size distributions depending on the energy dissipation rate (Martínez-Bazán et al., 1999b). Such information is used in the model presented by Martín et al. (2008b), Pohorecki et al. (2001a, b). It describes the equilibrium between the processes of coalescence and breakup of bubbles in the turbulent field.

In this model the coalescence rate in the mixer may be described by Eq. (7) and is equal to the product of collision frequencies θ_{ij}^T and their effectiveness $\lambda_{i,j}$

$$C_{ij}^T = \lambda_{ij} \cdot \theta_{ij}^T \tag{7}$$

where the collision frequency θ_{ij}^T is described by Eq. (8)

$$\theta_{ij}^T = n_i \cdot n_j \cdot \left[\frac{\pi}{16}\left(d_i + d_j\right)^2\right] \cdot \sqrt{u_i^2 + u_j^2} \tag{8}$$

The velocity of bubble u_i with diameter d_i is connected with turbulent energy dissipation rate by Eq. (9)

$$u_i = 1.4 \cdot \varepsilon^{1/3} \cdot d_i^{1/3} \tag{9}$$

Following the assumptions of the model, the latter quantity, i.e. effectiveness of bubble collisions $\lambda_{i,j}$ occurring in Eq. (7), amounts to

$$\lambda_{ij} = exp\left[\frac{ln\left(\frac{h_0}{h_f}\right) \cdot \sqrt{\frac{0.5 \cdot d_{ij} \cdot \rho_L}{16 \cdot \sigma}}}{\frac{\left(0.5 \cdot d_{ij}\right)^{2/3}}{\varepsilon^{1/3}}}\right] \tag{10}$$

where $d_{ij} = \left(\frac{2}{d_i} + \frac{2}{d_j}\right)^{-1}$, $h_0 = 1 \times 10^{-4}$ m, $h_f = 1 \times 10^{-8}$ m.

In the case of the gas bubble breakup, the rate of this process is described by Eq. (11) in its form similar to Eq. (7)

$$B_i = \kappa_i \cdot \theta_{ie} \tag{11}$$

Now the frequency of the collisions of bubbles with diameter d_i and eddies with diameter d_e reaches

$$\theta_{ie} = n_i \cdot n_e \cdot \left[\frac{\pi}{16}\left(d_i + d_j\right)^2\right] \cdot \sqrt{u_i^2 + u_e^2} \tag{12}$$

and the bubble velocity is given by equation

$$u_e = 1.4 \cdot \varepsilon^{1/3} \cdot d_e^{1/3} \tag{13}$$

The eddy colliding with a bubble must have an appropriate size and energy to break it up. The probability of the bubble breakup is the highest when $d_e = 0.6 \cdot d_i$. The amount of eddies sized d_e referred to the mass unit may be calculated from equation as follows

$$\frac{dN_e(k)}{dk} = 0.1\frac{k^2}{\rho_L} \tag{14}$$

with the wave number k defined as

$$k = \frac{2}{d_e} \tag{15}$$

The ratio of eddies having the energy sufficient to break a bubble up is described by Eq. (16)

$$\kappa_i = exp\left(-\frac{\frac{We_C \cdot \sigma}{d_i \cdot \rho_L}}{u_e^2}\right) \tag{16}$$

An important and final element of the model is a function G_i which presents an equilibrium between the processes of coalescence and breaking up for each size class

$$G_i = \frac{1}{2}\sum_{k=1}^{N}\sum_{l=1}^{N} C_{i,jk} - \sum_{j=1}^{N} C_{ij} + 2 \cdot B_m - B_i \tag{17}$$

where

$$C_{i,jk} = \begin{cases} C_{kl} \; if \; v_k + v_l = v_i \\ 0 \; if \; v_k + v_l \neq v_i \end{cases} \tag{18}$$

and B_m - breakup rate for m-class of bubbles ($v_m = 2 \cdot v_i$). For the known values of bubble concentrations (calculated according to Eq. (4)) and experimentally determined energy dissipation rates we can calculate the values of function G. If the model describes well the conditions prevailing in the mixer, the values of this function should be close to zero. However, to use the model we have to know the energy dissipation rate. Generally, the local energy dissipation rate may be calculated from the definition formula (Baldi et al., 2002; Delafosse et al., 2011; Tanaka and Eaton, 2007)

$$\varepsilon = \nu \cdot \overline{\frac{\partial u'_j}{\partial x_i} \cdot \left(\frac{\partial u'_i}{\partial x_j} + \frac{\partial u'_j}{\partial x_i}\right)} = \frac{1}{2} \cdot \nu \cdot \overline{\left(\frac{\partial u'_i}{\partial x_j} + \frac{\partial u'_j}{\partial x_i}\right)^2} \tag{19}$$

whereas for the mixer case the Eq. (20) is obtained

$$\varepsilon = \nu \cdot \left\{ \begin{array}{l} 2 \cdot \left[\overline{\left(\frac{\partial u'_t}{\partial x}\right)^2} + \overline{\left(\frac{\partial u' r}{\partial r}\right)^2} + \overline{\left(\frac{\partial u' z}{\partial z}\right)^2} \right] + \\ + \overline{\left(\frac{\partial u'_t}{\partial r}\right)^2} + \overline{\left(\frac{\partial u'_r}{\partial x}\right)^2} + \overline{\left(\frac{\partial u'_t}{\partial z}\right)^2} + \overline{\left(\frac{\partial u'_t}{\partial x}\right)^2} + \overline{\left(\frac{\partial u'_r}{\partial z}\right)^2} + \\ + \overline{\left(\frac{\partial u'_z}{\partial r}\right)^2} + 2 \cdot \left(\overline{\frac{\partial u'_t}{\partial r} \cdot \frac{\partial u'_r}{\partial x}} + \overline{\frac{\partial u'_t}{\partial z} \cdot \frac{\partial u'_z}{\partial x}} + \overline{\frac{\partial u'_r}{\partial z} \cdot \frac{\partial u'_z}{\partial r}} \right) \end{array} \right. \tag{20}$$

In measurements using the PIV system, velocity components are usually obtained only for two directions, whereas to use Eq. (20) it is necessary to introduce additional assumptions enabling the calculation of the missing elements. With the known radial and axial velocities, the assumption of the turbulence isotropy allows to calculate the turbulent energy dissipation rate from a simplified Eq. (21)

$$\varepsilon = \nu \cdot \left[2 \cdot \overline{\left(\frac{\partial u'_r}{\partial r} \right)^2} + 2 \cdot \overline{\left(\frac{\partial u'_z}{\partial z} \right)^2} + 3 \cdot \overline{\left(\frac{\partial u'_r}{\partial z} \right)^2} + 3 \cdot \overline{\left(\frac{\partial u'_z}{\partial r} \right)^2} + 2 \cdot \overline{\frac{\partial u'_r}{\partial z} \cdot \frac{\partial u'_z}{\partial r}} \right] \tag{21}$$

As indicated by our previous research (Rzyski and Stelmach, 2002; Stelmach, 2002), for the self-aspirating disc impeller the turbulence isotropy condition in the mixer is met, except for a small area close the impeller neighborhood.

However, the above presented simplification in form of Eq. (21) gives exact results if the distance between the measured velocity vectors is close to the local Kolmogorov spatial scale (Tanaka and Eaton, 2007). During the measurements carried out by the PIV system the distance between the vectors is strictly connected with the interrogation area. Most frequently, the practical, achievable distances between the measured velocity vectors are many times higher than the Kolmogorow scale. To obtain correct results, the assumptions using different turbulence models are applied. Quite popular in this respect became the Smagorinski model (Joshi et al., 2011; Micheletti et al., 2004), in which the turbulent energy dissipation rate may be calculated from Eq. (22)

$$\varepsilon = (C_S \cdot \Delta l)^2 \cdot \overline{\left[\frac{1}{2} \cdot \left(\frac{\partial u'_i}{\partial x_j} + \frac{\partial u'_j}{\partial x_i} \right)^2 \right]^{3/2}} \tag{22}$$

where Δl is a distance between velocity vectors resulting from the use of the PIV method. However, this method is inconvenient as it requires the Smagorinski constant C_s. Usually a value $C_s = 0.17$ is assumed, but values from 0.11 to 0.21 (de Jong et al., 2009; Kleissl, 2004; Sheng et al., 2000) also were applied.

The aim of the research is to check the usefulness of the presented model to describe the sizes of gas bubbles dispergated by the self-aspirating disc impeller with the values of modified Froud's number higher than the critical value. If the model is considered to be correct it will allow to determine the bubble size distributions in the mixer merely according to energy dissipation rate measurements.

For this purpose we should analyse:

- sizes of eddies capable of breaking up the bubbles of specific sizes;
- velocities of gas bubbles moving in liquid;
- values of local energy dissipation rates in the mixer.

2. EXPERIMENTS

The studies were carried out in a glass flat-bottomed tank with diameter $T = 0.292$ m, equipped with four $B = 0.1 \cdot T$ wide baffles. The self-aspirating disk impeller having the $D = 0.125$ m diameter was placed at the height of $h = 0.078$ m above the tank bottom. The tank was filled with distilled water containing tracer (seed) particles of 10 μm mean diameter to the $H = T$ level. To reduce optical deformations the cylindrical tank was immersed in a cuboidal tank filled with pure water. Velocity was measured at the impeller's rotational frequency $N = 6$ s^{-1} (360 min^{-1}) in the plane determined by the impeller's rotation axis and angle bisector between the baffles (Fig. 4). Under experimental conditions the Reynolds number reached the value $Re = 93580$, whereas the modified Froude number $Fr' = 0.258$. Under these conditions the gas hold-up amounts approximately to $\Phi = 0.43\%$ (Stelmach, 2000). With this content of gas in liquid the system may still be treated as monophasic. Due to the importance of the area just behind the blade of the impeller in which the gas bubbles are subjected to direct effects of eddies formed behind the blade the measurements were carried out for four angular positions of the blade in relation to the measurement plane at distances 0°, 5°, 10° and 15° behind the blade.

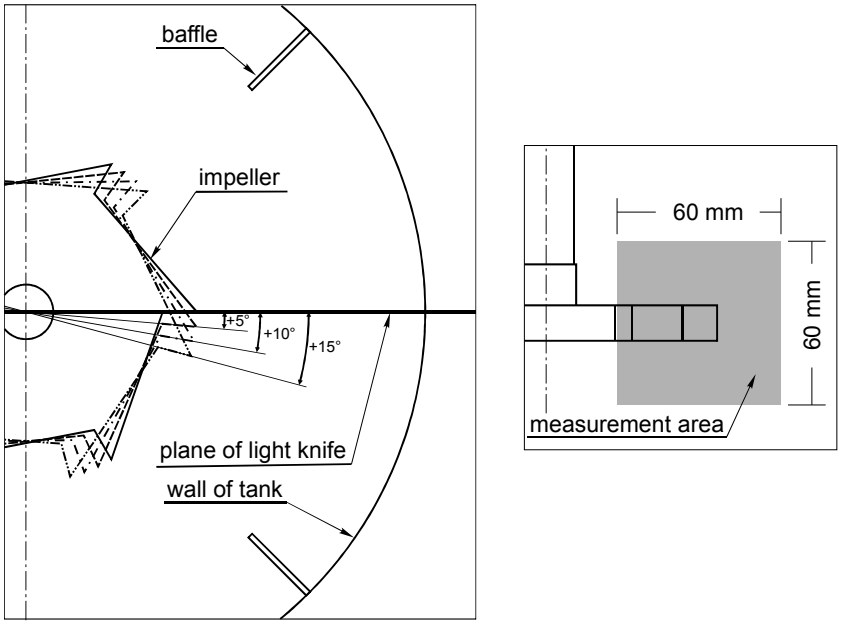

Fig. 4. Scheme of the measuring system

We used in the measurements the PIV measuring system made by *LaVision* company with double-pulsed laser of the maximum power 135 mW and *ImagePro* camera, 2048 px × 2048 px resolution, *Nikkor* 1.8/50 lens with a aperture (diaphragm) stopped down to the value assuring the maximum resolution (www.optycne.pl), i.e. the aperture number reached 5.6. The measurement area was sized approximately 60 mm ×60 mm. For each angle position of blade, 200 double photographs in about 33.3 s were made, with the $\Delta t = 415$ μs time interval between impulses (this interval was calculated for tracer displacement 10 px and velocity $0.3 \cdot \pi \cdot D \cdot N$). Laser impulses were synchronised with the blade passing through the measurement area plane by the use of external trigger (on the frames always the same blade is visible because the blade passing frequency was less than 15 Hz which is maximum registration frequency of apparatus). For data processing *DaVis 7.2* software was employed. Double data processing was used, with the final size of the interrogation area 32 px × 32 px (i.e. about 0.93 mm × 0.93 mm) without overlapping.

3. DISCUSSION OF RESULTS

3.1. Energy dissipation rate

Previous studies of energy spectrum of eddies (Stelmach et al, 2003) have shown the existence of an inertial sub-range almost the entire volume of tank with a self-aspirating disk impeller. So, the turbulent energy dissipation rate was calculated from the Smagorinski model (Eq. (22)) for $C_s = 0.11$ (Stelmach, 2014). *MathCAD* was used for calculations. Tabulated data of velocity pulsations were numerically differential (Panow, 1955). Since the unequivocal experimental method for determination of the energy dissipation rate it is not known obtained values were not corrected. It was found (Stelmach, 2014) that the local distributions of energy dissipation rates calculated from the Smagorinski model are very close to those calculated from the relationship $\varepsilon = C \cdot u'^3 / D$. The biggest differences in the values are observed in areas where isotropic turbulence condition is not met. The obtained contour plots (maps) of the distributions of local turbulent energy dissipation rates ε are presented in Fig. 5. Due to the effect of obscuring the measurement area by the blade, it was not possible for the applied measuring apparatus setting to determine value ε in the cavern just behind the blade.

The highest values ε occur in the middle of the impeller height at a distance of several millimeters from the blade edge. For the experimental conditions, $\varepsilon_{max} \approx 25$ m^2/s^3 was achieved at 15° angular distance. This value is approx. 90 times higher than the mean value for the whole liquid contained in the mixer which is equal to $\varepsilon_m = 0.267$ m^2/s^3 calculated based on the power consumption (Stelmach, 2000). Changes in the measuring plane position in respect to the impeller blade affect a value of ε only up to the distance of several millimeters from the impeller blade tip (Fig. 5). Therefore, the mean values of energy dissipation rate for the analyzed area vary from 6 to 7 m^2/s^3, depending on the blade position and this is about 25 times more than the mean value for the whole mixer. Consequently, near the impeller most of the energy is supplied by the impeller to the liquid. Instead, beyond that area the energy dissipation rate decreases rapidly.

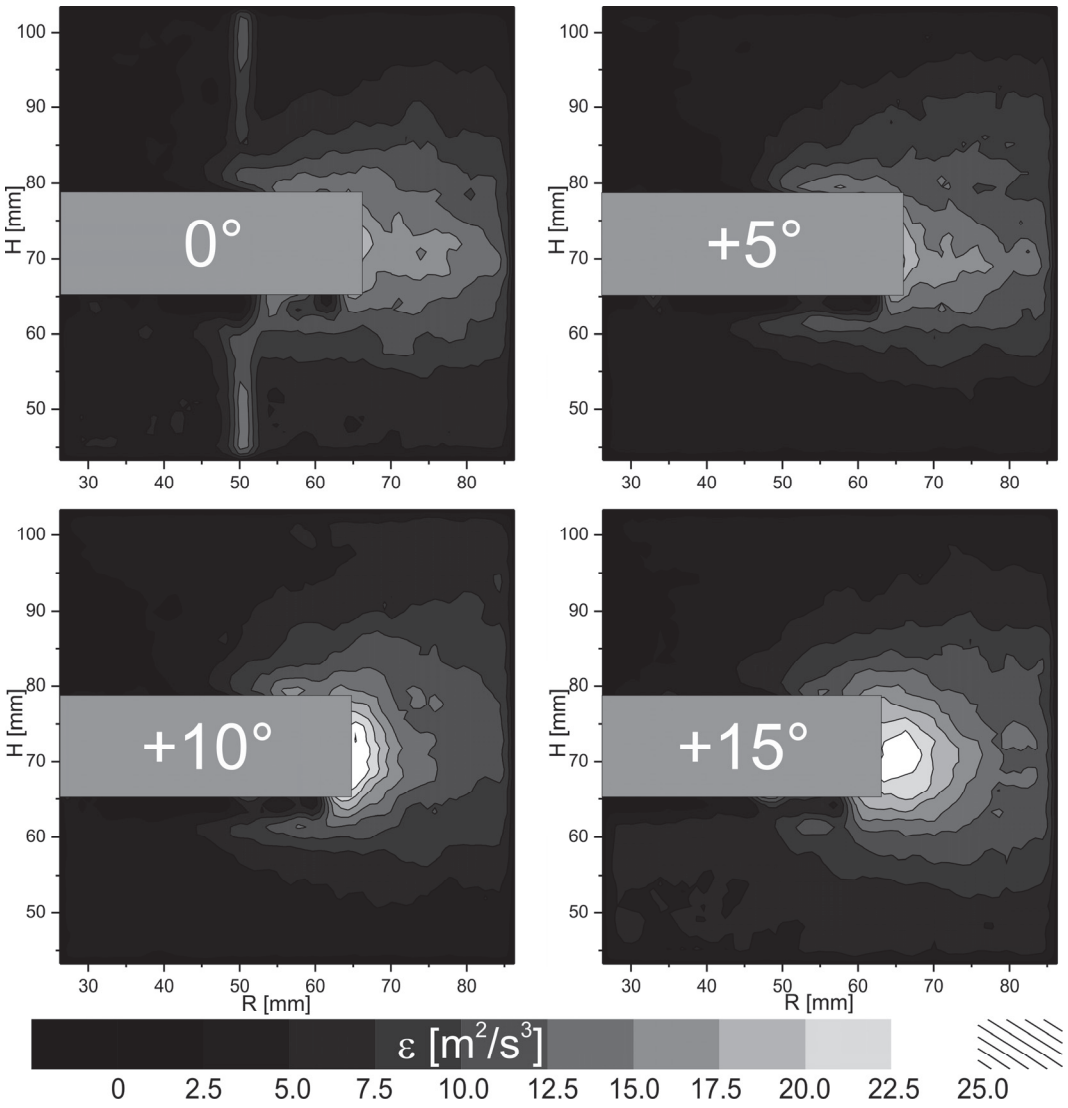

Fig. 5. Energy dissipation rate

3.2. Kolmogorov and Taylor eddy scales

Sizes of the smallest air bubbles should not be smaller than the Kolmogorov spatial scale

$$\eta = \left(\frac{\nu^3}{\varepsilon} \right)^{0.25} \tag{23}$$

The lowest value for this scale, calculated from Eq. (23) for a value of $\varepsilon_{max} = 25$ m^2/s^3, reaches in the discussed case approx. 0.014 mm. Analysis of Fig. 3 indicates that the sizes of the most numerously occurring bubbles established from the experiments are many times higher than that value.

We should also notice that a value of η obtained from Eq. (23) is over 60 times higher than the distance between velocity vectors in the PIV method. This extorts the necessity to use the Smagorinski model to calculate the energy dissipation rate according to the PIV measurements. Due to the required size of eddies which are capable of breaking gas bubbles up we can expect their similarity with the Taylor linear scale determining the onset of the dissipative area. Fig. 6 presents the contour plots of Taylor eddy size distributions calculated according to Eq. (24) (Baldi and Yianneskis, 2003).

$$\varepsilon = 30 \cdot \nu \cdot \frac{\overline{u'^2}}{\lambda_f^2} \tag{24}$$

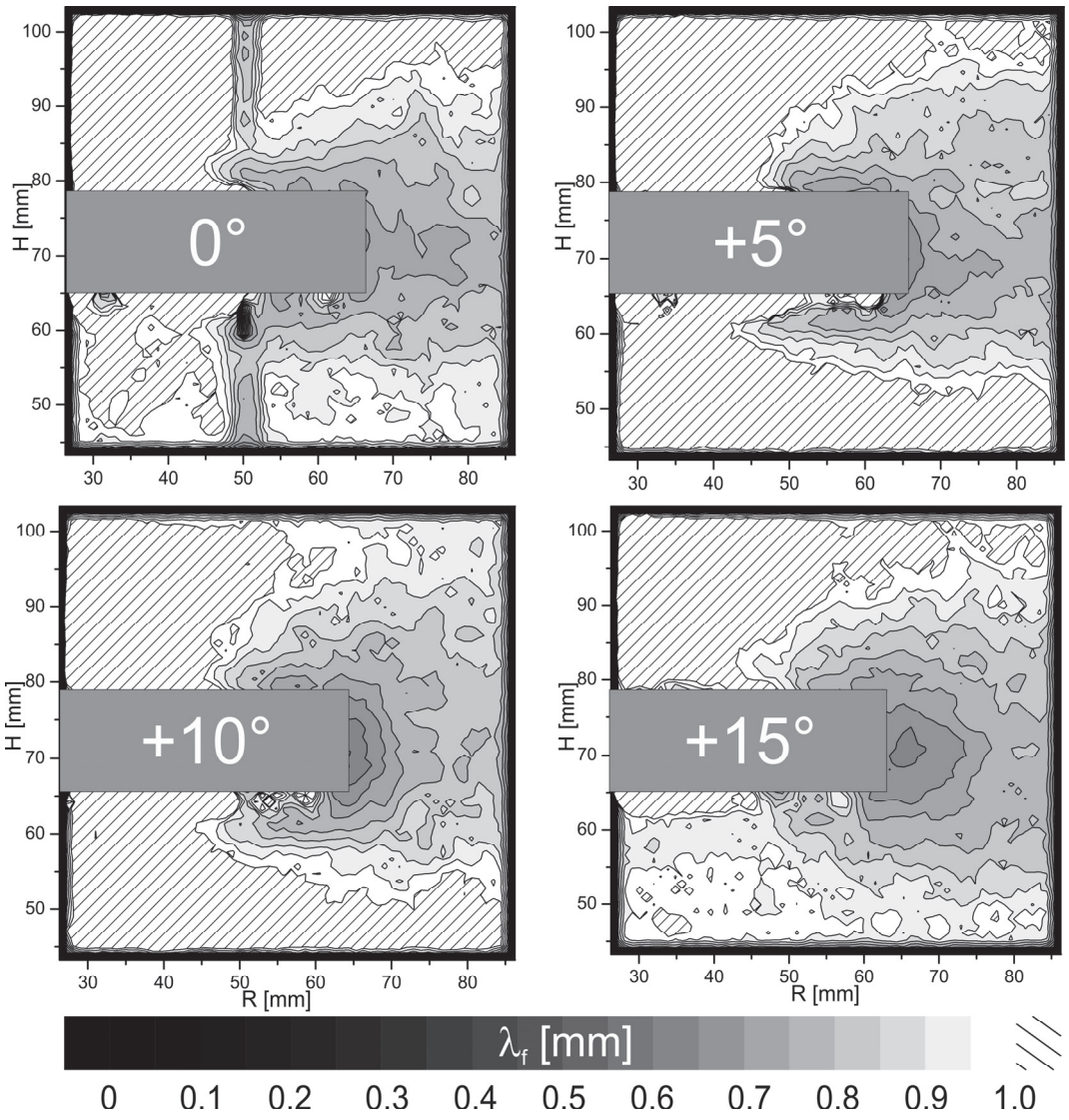

Fig. 6. Taylor eddy sizes

As results from analysis of Fig. 6, near the impeller the Taylor eddy sizes vary within a small range from approx. 0.6 mm to 1 mm and the obtained range of changes coincides well with experimental distribution of gas bubble diameters shown in Fig. 3. However, comparing Fig. 3 with Fig. 6 we can notice that for water the sizes of the most numerous bubbles are approx. twice smaller than the sizes of the smallest Taylor eddies behind the impeller blade.

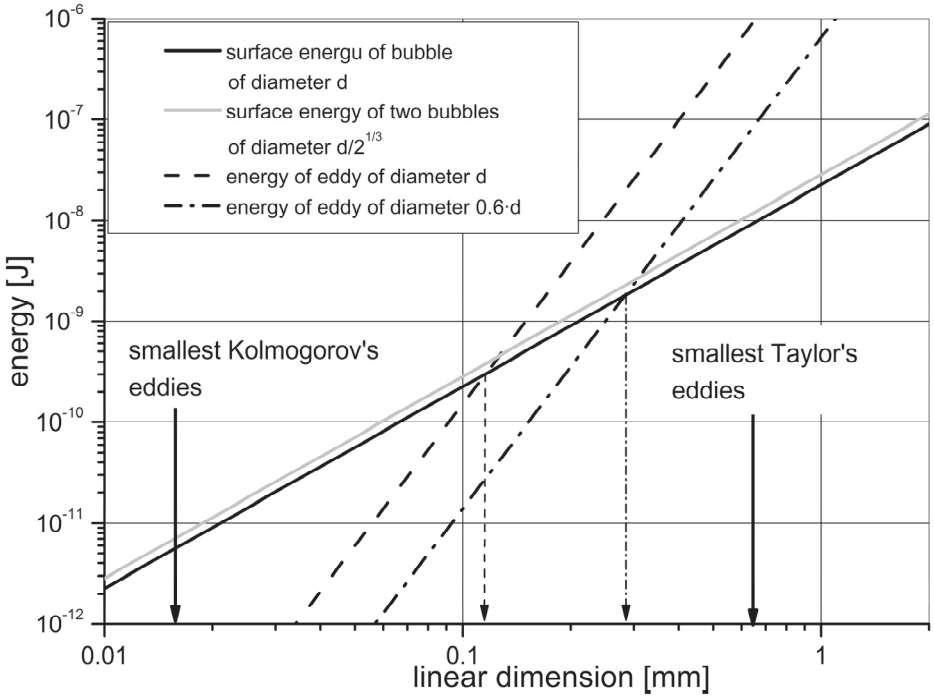

Fig. 7. Surface energy of bubbles and energy of eddies

As we have mentioned, eddies bigger than gas bubbles only shift them in liquid, whereas very small eddies actually do not interact with the bubbles. To break the bubble up the eddy size should range from 0.2 to 1 of the bubble diameter (Martín et al., 2008b), whereas its energy must be higher than the bubble surface energy. Therefore, subjected to profound analysis should be the bubble surface energies and energies of eddies exhibiting sizes equal to the size of the bubble or smaller. The previous studies (Stelmach et al., 2005) demonstrated that for the tested impeller in eddy energy spectrum there is a range of wave numbers where the Kolmogorov „-5/3" law is met (inertia range).

$$E(k) = \alpha \cdot \varepsilon^{2/3} \cdot k^{-5/3} \tag{25}$$

So if a value of ε is known, we can calculate energy of eddy with diameter $d = 2/k$ (Eq. (15)) and compare it with the surface energy of bubble $E_p = \frac{\pi \cdot d^2}{4}\sigma$ having the same diameter. The comparison of bubble surface energy and eddy energy is presented in Fig. 7.

The total surface energy of the bubbles arising from breaking up a bigger bubble is always higher than the surface energy (larger total surface). Fig. 7 compares also the surface energy exhibited by two bubbles of identical diameters and total volume equal to the volume of the broken up bubble. The figure presents also the ratio of the energy of eddies with diameter equal to 0.6 bubble diameter (Martín et al., 2008b). Analysis of Fig. 7 demonstrates that eddies sized less than 0.11 mm exhibit too low energy to break the bubbles up. This does not mean that the liquid will not contain any bubbles of smaller diameters, because they may occur while bigger bubbles are broken up. The course of the lines in Fig. 7 shows that for bigger bubbles and eddies the difference between the surface energy and the energy of the eddy increases. It is easier to break up the bubble then, especially because not all energy of the eddy must be consumed to break the bubble up (complete use of the eddy's energy is tantamount to disappearance of the eddy structure).

Figures 1b and 1c taken just behind the impeller blade show gas structures sized from several to a dozen millimeters (length of the blade in the figure – approx. 13 mm). On the other hand, the size of the greatest eddies meeting the „-5/3" law, calculated according to the energy spectrum density curve (Stelmach et al., 2003), amounts to about 8.5 mm. However, eddies bigger than that size also have sufficient energy to break the bubbles up (Fig. 7), and at a small concentration of the bubbles the

probability of the bubble collision with the eddy capable of breaking it up is high. In the case of big bubbles, the eddies capable of breaking them up have quite a high excess of energy, which gives rise to small bubbles sized even as fine as 0.15 to 0.25 mm.

3.3. Gas bubble size

For the adopted parameters of the impeller operation the mean value of the energy dissipation rate amounts to $\varepsilon_m = 0.267$ m^2/s^3. Substituting this value to Eq. (2), the mean Sauter diameter of the bubble $d_{32} = 5.5$ mm is obtained for water. Using the corrections introduced by Calderbank (Martín et al., 2008b) we reduce its value to $d_{32} = 5.2$ mm, although these values continue to be much higher than the experimental values presented in Fig. 3. Similarly as the Sauter diameter calculated from Eq. (3) for $C_2 = 0.6$ and $We_C = 1.2$ (Martín et al., 2008b) the Sauter diameter equal to $d_{32} = 2.45$ mm remains to be approx. 1.5 times higher than the measured value (Fig. 3). A high compatibility of experimental and theoretical value d_{32} is obtained only when for calculations the energy dissipation rate value 3 times higher than the mean value for the whole mixer is adopted, i.e. about $\varepsilon = 0.8$ m^2/s^3. This may result from the fact that in the areas largely distanced from the impeller the liquid turbulence drops fast. There are no bubbles breaking up process there, but the volume of that liquid significantly affects the mean value ε. Therefore, for the areas e.g. near the impeller where the bubble is actually broken up, it should be more appropriate to use in these calculations the local values of energy dissipation rate. This may also solve another problem connected with the use of equation of type (2) for self-aspirating impellers. Increasing the impeller rotational frequency causes an increase in the area of consideration, so also an increase in the mean velocity of energy dissipation, and pursuant to Eq. (2), Sauter diameters should be decreasing. Actually, for self-aspirating impellers a reverse phenomenon (Stelmach, 2007) is observed, as depicted in Fig. 3. This phenomenon may be explained by the fact that with increasing rotational frequency of the impeller not only the power consumption increases, but also the amount of the aspired gas. The increased size of the interfacial area decreases in turn the liquid turbulence and both inflows are partly reduced. There is no such effect when gas is supplied by the sparger, where the amount of gas in the mixer does not depend on the impeller rotational frequency. Therefore, the usefulness of a relation of type (2) in predicting the sizes of the bubbles dispersed by self-aspirating impellers is largely limited.

3.4. Bubble velocities

Determination of the distributions of energy dissipation rates allows to check the usability of Eq. (9) determining the gas bubble movement velocity in the turbulent field generated by the self-aspirating disc impeller. Figure 8 presents the contour plots of bubble velocities with different diameters d_b calculated from Eq. (9) for the 15° measurement cross-sectional position behind the blade.

In the case of a mixer the experimental determination of the resultant bubble velocities having fixed diameters is very difficult. In the previous studies (Stelmach, 2014) the mean relative bubble velocities without division into fractions were determined. The obtained results are presented in Fig. 9.

A comparative analysis of Figs. 8 and 9 allows to state that the calculated values of bubble velocities are within the measured velocities. This enables adopting Eq. (9) for further calculations.

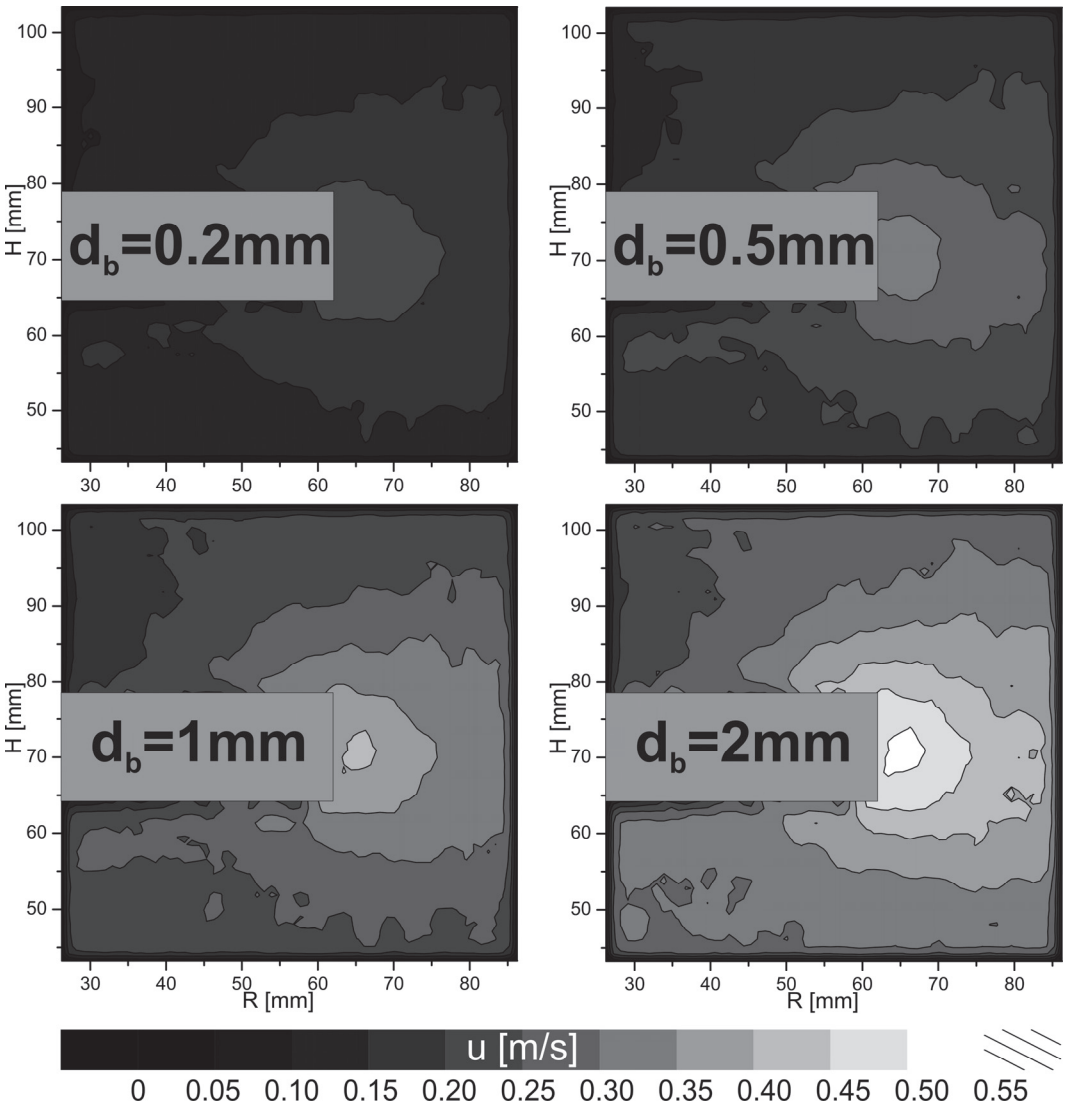

Fig. 8. Bubble velocities calculated from Eq. (9)

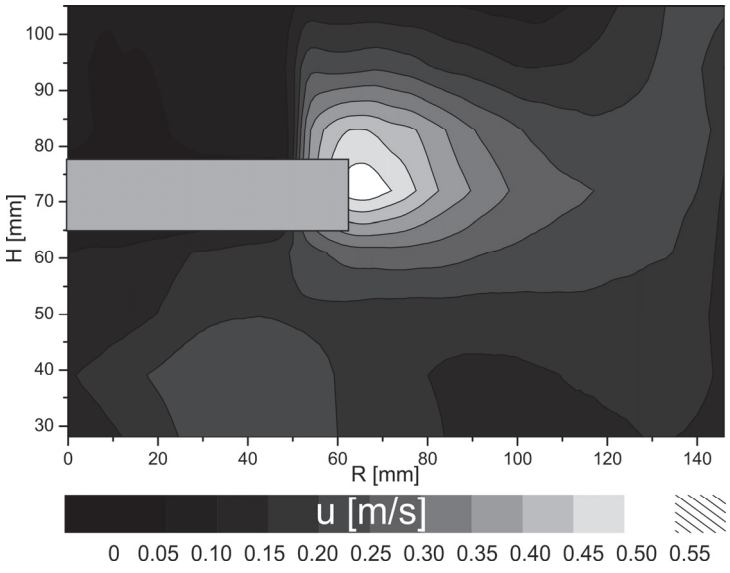

Fig. 9. Bubble velocities determined experimentally for $N = 360$ min^{-1}

3.5. Results of model calculations

The usefulness of the mathematical model described in the introduction and used to predict gas bubble sizes according to local velocities of energy dissipation was checked with the following simplifying assumptions:

- the bubble is broken up by an eddy with the diameter equal to 0.6 of the bubble diameter (centre of the range 0.2 - 1 (Martín et al., 2008b)),
- the bubble is broken up into two bubbles of equal volumes, which means that $d_{i\text{-}1}=\frac{d_i}{\sqrt[3]{2}}$,
- the number of the bubbles in 1 m^3 amounts to 1.79×10^7 and 2.99×10^7.

The number of the bubbles in 1 m^3 of the liquid was determined according to analysis of photographs which were used to determine experimental distributions of bubble sizes presented in Fig. 3. The photographs comprised 1/4 of the mixer transverse intersection, whereas the thickness of the illuminated layer of water reached about 1 cm. This allowed to determine the volume in which bubble images were counted. The minimum and maximum registered number of the bubbles was used in calculations.

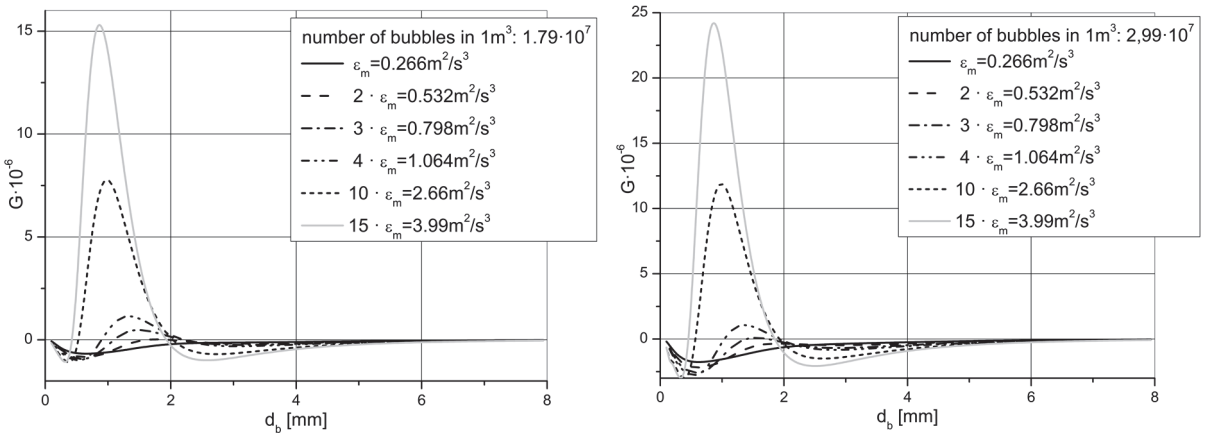

Fig. 10. Values of function G, depending on the size and number of the bubbles

As the energy dissipation rate close to the mixer is many times higher than its value for the whole mixer ε_m = 0.266 m^2/s^3, the calculations of a value of function G from Eq. (17) were carried out using the *MathCAD* package for several multiplicities of ε_m. The calculations were made using Eqs. (7) - (18). The results obtained are presented in Fig. 10.

As it results from analysis of Fig. 10, the greatest influence on the values of function G was that of energy dissipation rate. On the other hand, the influence of the number of bubbles is noticeable, but it did not change the course of the function (shape of the curve). Function G expresses an equilibrium between the processes of breaking up and coalescence and for the steady state in which the bubble size distributions were determined, its value should be zero. For a value of $\varepsilon \approx 0.8$ m^2/s^3, i.e. for such areas in the mixer where $\varepsilon < 3\cdot\varepsilon_m$, we can speak about relatively insignificant deviations in the value of function G from zero (as compared to its maximum values), and the verified model may be considered useful. However, near the impeller, in which much higher values of energy dissipation rate are observed (Fig. 5) along with a relatively high share of small-sized eddies, the model is ineffective. The lack of compatibility should be probably attributed to the mechanism of breaking up big bubbles while they are leaving the impeller orifices. Analysis of photographs (Fig. 1 and 2) suggests that the gas bubble is torn off the gas bubble surface inside the impeller and the size of this bubble may reach the size of the outlet orifice. At the further stage it is broken up into smaller bubbles, because at greater distances from the impeller they are no longer so big. However, for a big bubble to be broken up, high energy eddies are needed. Analysis of Fig. 7 shows that for the tested self-aspirating impeller the eddies

of appropriate sizes and energies occur in that area and such breaking up process becomes possible. However, such process does not have to be consistent with the model assumption about breaking each bubble up into two bubbles of equal size and the hitherto collected data do not allow to advance an explicit thesis about the mechanism of breaking up each bubble. For this purpose it is necessary to make a sequence of pictures (film) at an approximate rate of 1000 frames per second.

At a further stage of the research some iterative calculations were made, which consist in determination of a model distribution of bubble sizes for which function G is zero. The calculations were made for $\varepsilon = 15 \cdot \varepsilon_m = 4$ m^2/s^3 and $\varepsilon = 25 \cdot \varepsilon_m = 6.68$ m^2/s^3. The latter value is close to the mean value of the energy dissipation rate in the interrogation area. A comparison of the experimental (Eqs. (4-6)) and calculated curves of the bubble size distribution at the impeller level is presented in Fig. 11.

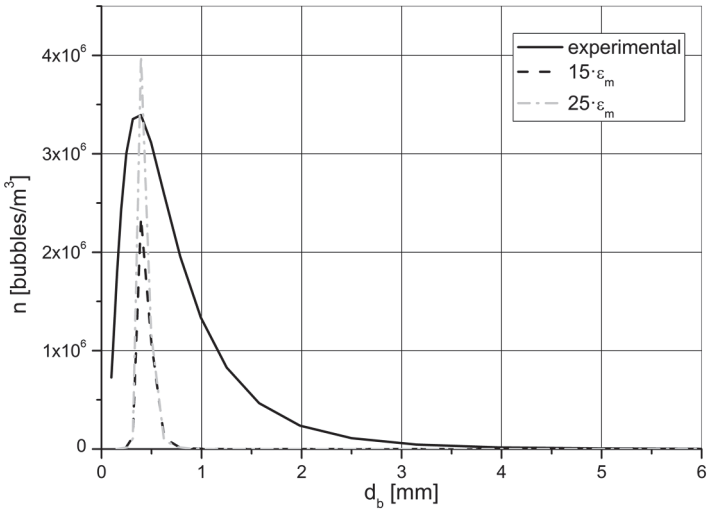

Fig. 11. Curves of the bubble size distribution at the impeller level

Analysis of curves in Fig. 11 indicates that the bubble size distribution calculated according to the model should be more monodispersive. On the other hand, the curves maxima achieved from the model solution and obtained according to experiments refer to the same bubble sizes and in this aspect the experiment positively verifies the model. A better compatibility was obtained for $\varepsilon = 25 \cdot \varepsilon_m$ value, i.e. that close to the mean value of the measurement area just behind the impeller blade.

The presented model yields promising results. However, the discrepancies between experimental and calculated distribution of bubble sizes suggest that the adopted simplifications are too gross. To be able to determine the distributions of bubble sizes for self-aspirating impellers according to the local velocities of energy dissipation, in my opinion further studies are necessary. Their primary purpose should be identification of the mechanism of big bubble break-up when leaving the outlet orifice. This may significantly diverge from the adopted consecutive division into two bubbles of equal volumes.

Verification of the model was based on independent measurements, separate for the movements of liquid phase and gaseous phase. More detailed data for the model verification should be derived from simultaneous measurements of liquid and bubble velocities. Such measurements with PIV method are feasible at low values of the gaseous phase hold-up Φ. Data obtained in this way should better suit the model assumptions.

4. CONCLUSIONS

The higher rotational frequency of the impeller increases not only liquid turbulence and power consumption but also the amount of aspired gas. The consequently enlarged interfacial area decreases

in turn liquid turbulence and both inflows are partly reduced. This results in the limited use of Eq. (2) to determine gas bubble size for self-aspirating impellers.

The experimentally determined sizes of gas bubbles exceed by several dozen times the sizes of the smallest eddies from the Kolmogorov range but largely coincide with the linear scale of the Taylor eddies.

The analysis indicates that despite some differences existing in hydrodynamics between the air-lift column and the mixer with self-aspirating impeller the gas dispergation model for the column may be adopted for the mixer design. However, there is still a demand for research aimed at the description of the phenomena occurring near the mixer outlet orifices.

The study was carried out within project no. W-10/1/2014/Dz.St.

SYMBOLS

B	baffle width, m
D	impeller diameter, m
d_b	gas bubble diameter, m (mm)
d_i	diameter of class i bubbles, m (mm)
d_{32}	Sauter mean diameter, m (mm)
E_p	surface energy of bubble, J
$E(k)$	density of eddy energy spectrum
g	gravitational acceleration, $m \cdot s^{-2}$
H	liquid level in the mixer, m
h	impeller distance from the bottom, m
k	wave number, m^{-1}
N	rotational frequency, s^{-1}
n_i	number of class i bubbles,
T	tank diameter, m
u	velocity, $m \cdot s^{-1}$
u_i	velocity of class i bubbles, $m \cdot s^{-1}$
u'	mean square pulsation of velocity (RMS), $m \cdot s^{-1}$

Subscripts

r, t, z	radial, tangential, axial

Greek symbols

α	Kolmogorov constant
ε	energy dissipation rate, $m^2 \cdot s^{-3}$
η	Kolmogorov spatial scale, m (mm)
λ	Taylor spatial scale, m (mm)
μ	coefficient of dynamic viscosity, Pa·s
ν	coefficient of kinematic viscosity, $m^2 \cdot s^{-1}$
ρ	density, $kg \cdot m^{-3}$
σ	surface tension, $N \cdot m^{-1}$

Dimensionless numbers

$Fr' = \frac{N^2 \cdot D^2}{g \cdot (H-h)}$	modified Froude number

$Re = \frac{N \cdot D^2 \cdot \rho}{\mu}$ Reynolds number

$We = \frac{N^2 \cdot D^3 \cdot \rho}{\sigma}$ Weber number

REFERENCES

Baldi S., Hann D., Yianneskis M., 2002. On the measurements of turbulence energy dissipation in stirred vessels with PIV techniques. *10th International Symposium on Applied of Laser Technique to Fluid Mechanics*. Lisboa, Portugal, 8-11 July 2002.

Baldi S., Yianneskis M., 2003. On the direct measurement of turbulence energy dissipation in stirred vessels with PIV. *Ind. Eng. Chem. Res*., 42, 7006-7016. DOI: 10.1021/ie0208265.

Delafosse A., Collignon M.-L., Crine M., Toye D., 2011. Estimation of the turbulent kinetic energy dissipation rate from 2D-PIV measurements in a vessel stirred by an axial Mixel TTP impeller. *Chem. Eng. Sci.*, 66, 1728-1737. DOI: 10.1016/j.ces.2011.01.011.

Deshmukh N.A., Patil S.S., Joshi J.B., 2006. Gas induction characteristics of hollow self-inducing impeller. *Chem. Eng. Res. Des.*, 84, 124-132. DOI: 10.1205/cherd05005.

de Jong J., Cao L., Woodward S.H., Salazar J.P.L.C., Collins L.R., Meng H., 2009. Dissipation rate estimation from PIV in zero-mean isotropic turbulence. *Exp. Fluids*, 46, 499-525. DOI: 10.1007/s00348-008-0576-3.

Evans G.M., Rielly C.D., Davidson J.F., Carpenter K.J., 1992. Hydrodynamic characteristics of a gas-inducing impeller. *Fluid Mechanics of Mixing*, 10, 153-161. DOI: 10.1007/978-94-015-7973-5_18.

Forrester S.E., Rielly C.D., Carpenter K.J., 1998. Gas-inducing impeller design and performance characteristics. *Chem. Eng. Sci.*, 53, 603-615. DOI: 10.1016/S0009-2509(97)00352-7.

Forrester S.E., Rielly C.D., 1998. Bubble formation from cylindrical, flat and concave sections exposed to a strong liquid cross-flow. *Chem. Eng. Sci.*, 53, 1517-1527. DOI: 10.1016/S0009-2509(98)00019-0.

Joshi J.B., Nere N.K., Rane C.V., Murthy B.N., Mathpati C.S., Patwardhan A.W., Ranade V.V., 2011. CFD simulation of stirred tanks: Comparison of turbulence models. Part I: Radial flow impellers. *Can. J. Chem. Eng.*, 89, 23-28. DOI: 10.1002-cjce.20446

Ju F., Cheng Z.-M., Chen J.-H., Chu X.-H., 2009. A novel design for a gas-inducing impeller at the lowest critical speed. *Chem. Eng. Res. Des.*, 87, 1069-1074. DOI: 10.1016/j.cherd.2009.01.009.

Kawase Y., Moo-Young M., 1990. Mathematical models for design of bioreactors: Applications of Kolmogoroff's theory of isotropic turbulence. *Chem. Eng. J.*, 43, B19-B41.

Kleissl J., 2004. *Field experimental study of the Smagorinsky model and application to Large Eddy Simulation*. PhD Thesis. Johns Hopkins University, Baltimore.

Kulkarni A.A., Joshi J.B., 2005. Bubble formation and bubble rise velocity in gas-liquid systems: A review. *Ind. Eng. Chem. Res.*, 44, 5873-5931. DOI: 10.1021/ie049131p.

Laakkonen M., Alopaeus V., Aittama J., 2002. The determination of parameters for bubble breakage and coalescence functions for gas-liquid systems in a mixed tank. *Annual Meeting Archive - American Institute of Chemical Engineers*, Indianapolis, United States.

Martín M., Montes F.J., Galán M.A., 2008. Bubbling process in stirred tank reactors I: Agitator effect on bubble size, formation and rising. *Chem. Eng. Sci.*, 63, 3212-3222. DOI: 10.1016/j.ces.2008.03.028.

Martín M., Montes F.J., Galán M.A., 2008. Influence of impeller type on the bubble breakup process in stirred tanks. *Ind. Eng. Chem. Res.*, 47, 6251-6263. DOI: 10.1021/ie800063v.

Micheletti M., Baldi S., Yeoh S.L., Ducci A., Papadakis G., Lee K.C., Yianneskis M., 2004. On spatial and temporal variations and estimates of energy dissipation in stirred reactors. *Chem. Eng. Res. Des.*, 82, 1188-1198. DOI: 10.1205/cerd.82.9.1188.44172.

Patil S.S., Joshi J.B., 1999. Stability of gas-inducing type impellers. *Can. J. Chem. Eng.*, 77, 793-803. DOI: 10.1002/cjce.5450770503.

Patwardahan A.W., Joshi J.B., 1999. Design of gas-inducing reactors. *Ind. Eng. Chem. Res.*, 38, 49-80. DOI: 10.1021/ie970504e.

Pohorecki R., Moniuk W., Zdrójkowski A., Bielski P., 2001. Hydrodynamics of a pilot plant bubble column under elevated temperature and pressure. *Chem. Eng. Sci.*, 56, 1167-1174. DOI:10.1016/S0009-2509(00)00336-5.

Pohorecki R., Moniuk W., Bielski P., Zdrójkowski A., 2001. Modeling of the coalescence/redispersion processes in bubble columns. *Chem. Eng. Sci.*, 56, 6157-6164. DOI: 10.1016/S0009-2509(01)00214-7.

Poncin S., Nguyen C., Midoux N., Breysse J., 2002. Hydrodynamics and volumetric gas-liquid mass transfer coefficient of a stirred vessel equipped with a gas-inducing impeller. *Chem. Eng. Sci.*, 57, 3299-3306. DOI: 10.1016/S0009-2509(01)00214-7.

Rigby G.D., Evans G.M., Jameson G.J., 1997. Bubble break up from ventilated cavities in multiphase reactors. *Chem. Eng. Sci.*, 52, 3677-3677. DOI: 10.1016/S0009-2509(97)00214-5.

Rzyski E., Stelmach J., 2002. Fluktuacje prędkości podczas mieszania cieczy nieniutonowskiej. *Inż. Ap. Chem.*, 41 (33), 4s, 113-115.

Sardeindg R.F., Poux M., Xuereb C., 2006. Development of a new gas-inducing turbine family: The partially shrouded turbine. *Ind. Chem. Eng. Res.*, 45, 4791-4804. DOI: 10.1021/ie051303a.

Sheng J., Meng H., Fox R.O., 2000. A large eddy PIV method for turbulence dissipation rate estimation. *Chem. Eng. Sci.*, 55, 4423-4434. DOI: 10.1016/S0009-2509(00)00039-7.

Stelmach J., 2000. *Badanie pracy samozasysającego mieszadła tarczowego*. PhD Thesis. Lodz University of Technology, Łódź (in Polish).

Stelmach J., 2002. Fluktuacje prędkości na wysokości samozasysającego mieszadła tarczowego. *Inż. Chem. Proces.*, 22, 3e, 1315-1320 (in Polish).

Stelmach J., 2006. Rozmiary pęcherzyków w początkowej fazie samozasysania. *Inż. Ap. Chem.*, 45, (37), 6s, 225-227 (in Polish).

Stelmach J., 2007. Rozkłady wielkości pęcherzyków gazu w początkowej fazie samozasysania. *Inż. Ap. Chem.*, 46 (38), 4-5, 117-119.

Stelmach J., 2014. *Hydrodynamika układu dwufazowego ciecz-gaz - Wykorzystanie metod fotooptycznych*. Monografie Politechniki Łódzkiej, Łódź.

Stelmach J., Kurasiński T., Kuncewicz Cz., 2005. Analiza porównawcza wybranych metod obliczania szybkości dyssypacji energii. *Inż. Chem. Proces.*, 26, 201-215 (in Polish).

Stelmach J., Rzyski E., Kania A., 2003. Energy dissipation on the level of a self-aspirating disk impeller. *11th Conference on Mixing*, Bamberg, October 2003, Germany.

Stręk F., 1981. *Mieszanie i mieszalniki.* WNT, Warszawa (in Polish).

Tan R.B.H., Chen W.B., Tan K.H., 2000. A non-spherical model for bubble formation with liquid cross-flow. *Chem. Eng. Sci.*, 55, 6259-6267. DOI:10.1016/S0009-2509(00)00211-6.

Tanaka T., Eaton J.K., 2007. A correction method for measuring turbulence kinetic energy dissipation rate by PIV. *Exp. Fluids*, 42, 893-902. DOI: 10.1007/s00348-007-0298-y.

Wang Z., Peng X., Li X., Wang S., Cheng Z., Ju F., 2013. Impact of liquid driving flow on the performance of a gas-inducing impeller. *Chem. Eng. Process. Process Intensif.*, 69, 63-69. DOI: 10.1016/j.cep.2013.02.009.

Zhang L., Shoji M., 2001. Aperiodic bubble formation from a submerged orifice. *Chem. Eng. Sci.*, 56, 5371-5381. DOI: 10.1016/S0009-2509(01)00241-X.

Zhang W., Tan R.B.H., 2000. A model for bubble formation and weeping at a submerged orifice. *Chem. Eng. Sci.*, 55, 6243-6250. DOI: 10.1016/S0009-2509(00)00215-3.

Received 03 July 2015
Received in revised form 18 August 2016
Accepted 30 August 2016